Supporting Information

Hot Holes Assist Plasmonic Nanoelectrode Dissolution

Alexander Al-Zubeidi[1§], Benjamin S. Hoener[1§], Sean S.E. Collins[1,3], Wenxiao Wang[2], Silke R. Kirchner[1], Seyyed Ali Hosseini Jebeli[2], Anneli Joplin[1], Wei-Shun Chang[1¶], Stephan Link[1,2,3], Christy F. Landes[1,2,3*]*

Rice University, [1]Department of Chemistry, [2]Department of Electrical and Computer Engineering, [3]Smalley-Curl Institute; 6100 Main Street; MS-60; Houston, TX 77005

* Corresponding authors, emails: slink@rice.edu, cflandes@rice.edu

§ Both authors contributed equally to this work.

¶ Present address: Department of Chemistry and Biochemistry, University of Massachusetts Dartmouth, 285 Old Westport Rd, North Dartmouth, MA 02747

1 Beam Spot Characterization

The beam spot was approximated as having an elliptical shape. A grid with a 50 micron spacing was created by cutting strongly scattering marks into the support using a focused ion beam (FIB).[1] The spacing between FIB marks was used as a ruler to estimate the beam size. For every experiment, a single-lens-reflex (SLR) camera image was taken of the beam spot and its size was calculated with respect to the FIB marked ruler using the 'imdistline' function in MATLAB to convert pixels into μm.

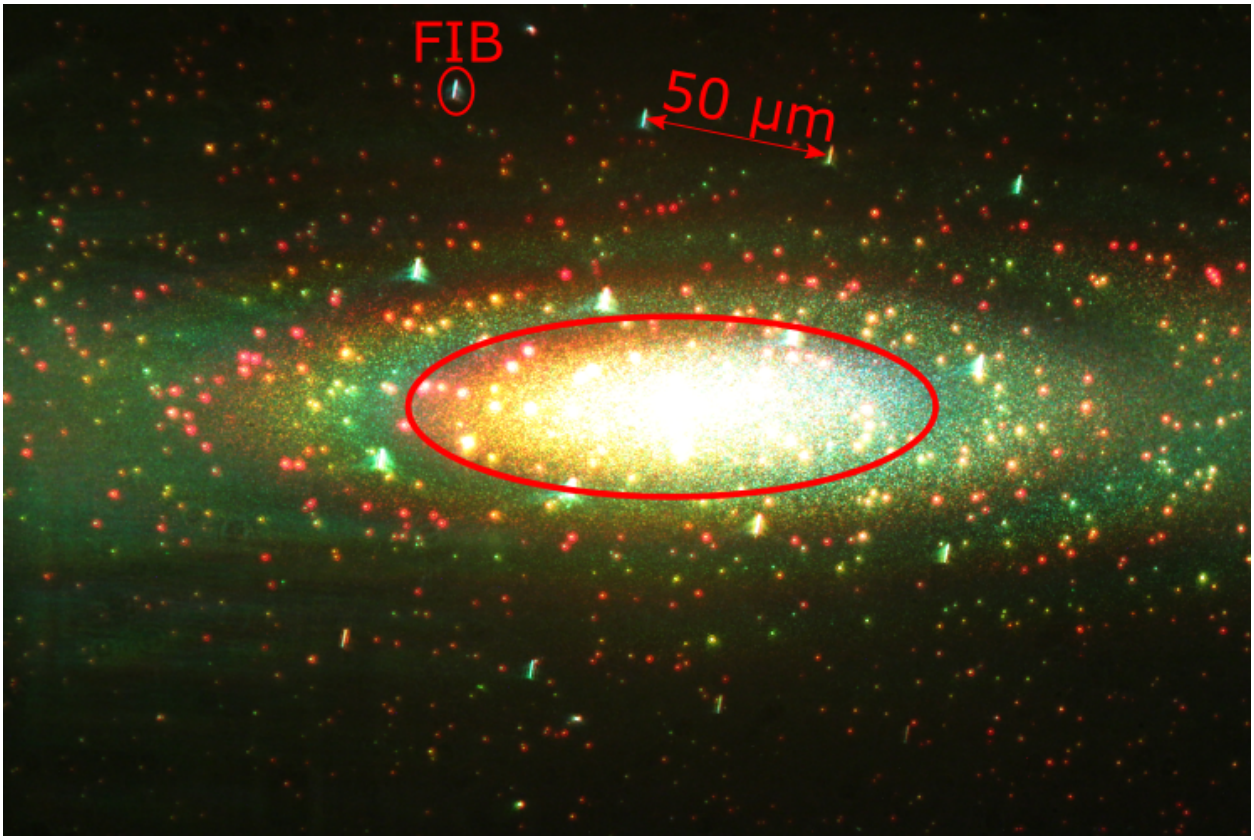

Figure 1. SLR camera image of the laser beam and FIB marked grid. The elliptical approximation of the total size of the beam spot is shown in red.

2 Electrochemical Cell Calibration

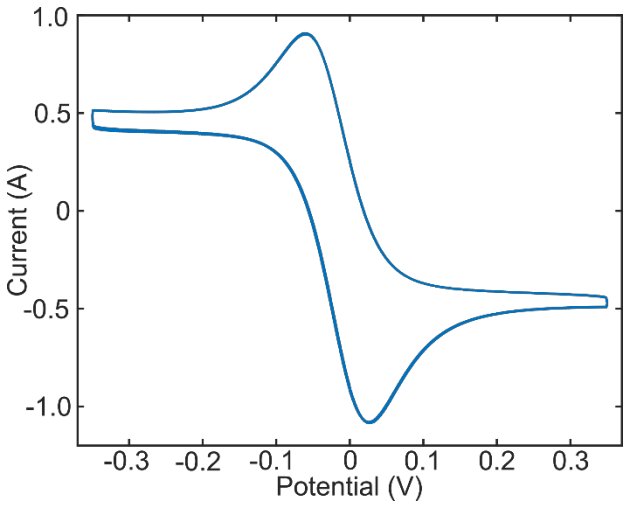

Figure 2. Bulk cyclic voltammetry (CV) for four cycles from -0.35 V to +0.35 V in a standard flow cell used for snapshot hyperspectral imaging with 500 mM NaCl electrolyte and 500 µM $K_4Fe(CN)_6$.

The Pt quasireference electrode was calibrated relative to a standard hydrogen electrode (SHE) using the ferri/ferrocyanide redox reaction. The average of the difference between redox peaks over four cycles, $E_0^{1/2}$, was -0.018 V. The $E_0^{1/2}$ value for the ferri/ferrocyanide redox couple has been reported as 0.211 V.[2] Therefore, 0.229 V was added to convert the measured potentials to values relative to the SHE potential. All values reported in the main text are given with respect to the SHE potential.

3 Supporting Information to Figure 1

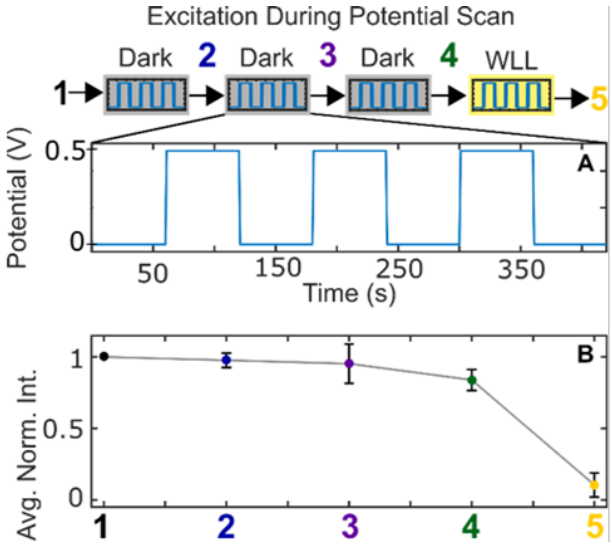

Figure 3. (a) The working electrode potential was cycled from 0 V to 0.5 V without (dark) and with white light laser excitation. Spectra and 0^{th} order intensities were taken before and after each cycle (1-5). (b) Average normalized 0^{th} order intensity from 20 gold nanorods before a potential is applied (1), after each potential cycle without white light laser excitation (2-4), and after a potential cycle with white light laser excitation (5). After three cycles in the dark, the scattering intensity had decreased only slightly, but after one cycle during illumination the mean scattering intensity dropped to 20% of its initial value.

4 Supporting Information to Figure 2

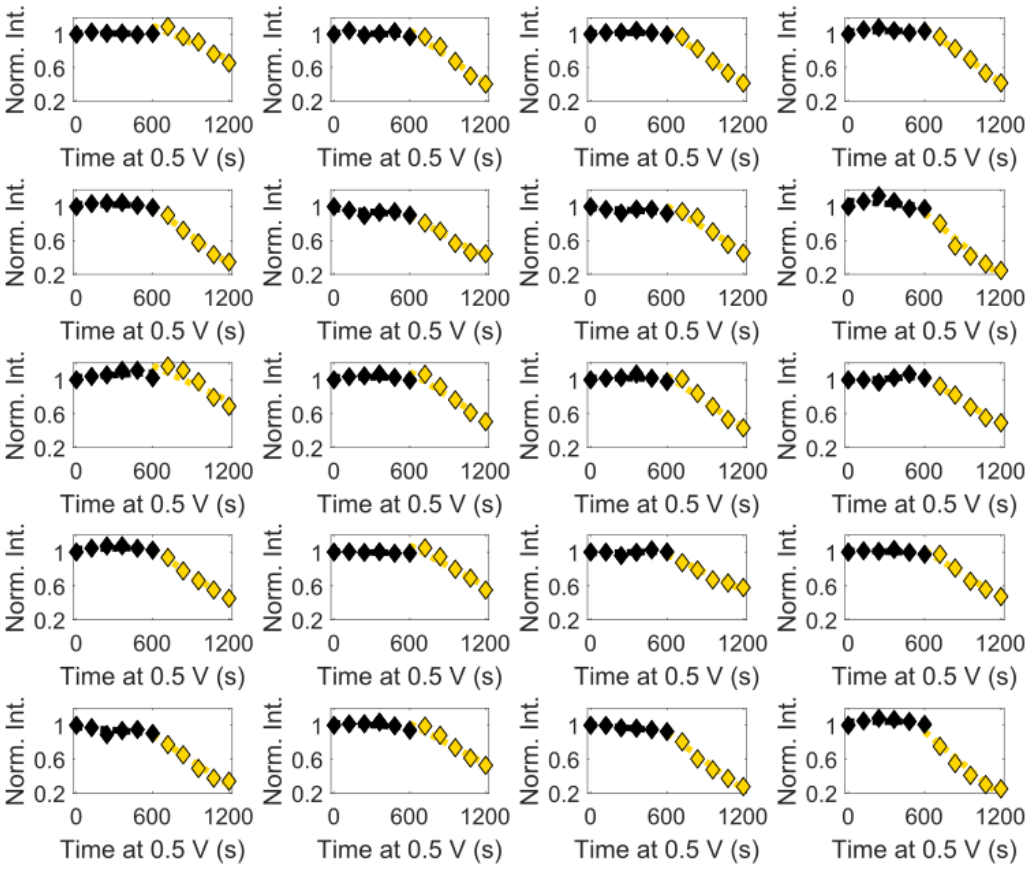

Figure 4. Change in scattering intensity recorded for single gold nanorods while cycling a 0.5 V electrochemical potential in the dark (black) and in the light (yellow), as illustrated in Fig. S3. Shown here is the data for all the single particles that were included in the analysis given in Figure 2b.

5 Light Assisted Electrochemical Dissolution of Gold Nanospheres

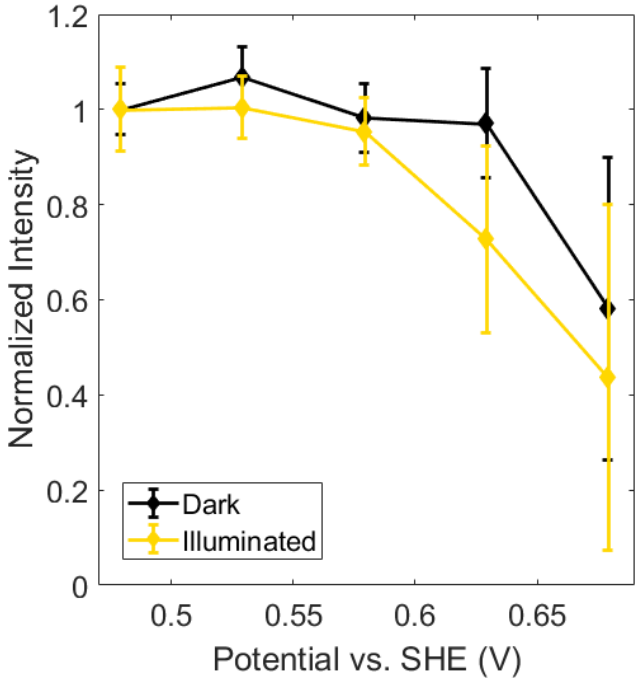

Figure 5. Average normalized scattering intensity of the same 70 nm gold nanospheres with and without white light excitation.

Dissolution of citrate stabilized gold nanospheres is also enhanced by optical excitation. Fig. S5 shows the average scattering intensity of 70 nm gold nanospheres collected after potential cycling within a range of 0 V to a maximum potential that was increased from +0.48 V to +0.68 V. The same nanospheres were first cycled to a maximum potential in the dark, and then monitored during light illumination at the same potential. The potential was then increased and the procedure was repeated. Almost no decrease in average scattering intensity was observed after cycling from 0 V to +0.63 V without excitation, while a ~30% decrease in intensity was observed for the same gold nanospheres after cycling to the same maximum potential with excitation using a halogen lamp.

6 Reaction Scheme

$$Au^0_{(s)} \underset{1}{\overset{2Cl^-}{\rightleftharpoons}} Au^0_{(s)}(Cl^-_{ads})_2 \xrightarrow[2]{-e^-} [Au^I Cl_2]^-_{ads} \underset{3}{\rightleftharpoons} [Au^I Cl_2]^-_{(aq)}$$

$$2\,Cl^- / -2e^- \Big\| 4$$

$$[Au^{III} Cl_4]^-_{(ads)} \underset{5}{\rightleftharpoons} [Au^{III} Cl_4]^-_{(aq)}$$

Scheme 1. Reaction mechanism based on bulk dissolution studies.

Based on previous research, chloride ions begin to adsorb onto gold nanorods at 0.48 V vs SHE (step 1).[3] Bulk dissolution studies suggest that gold dissolves by first forming $[AuCl_2]^-$ which can desorb (step 3) or further oxidize to $[AuCl_4]^-$ (step 4).[4, 5] The latter can desorb and go into solution (step 5). Studies of the equilibrium between $[AuCl_2]^-$ and $[AuCl_4]^-$ have found that depending on the conditions, both complexes can be stable in solution. The equilibrium is dependent on temperature, concentration of chloride ions, concentration of dissolved Au complexes, pH, and applied potential.[4-7] Furthermore, gold in its native state has been reported to act as a catalyst for interconversion between the two complexes.[4] Under neutral conditions, the inclusion of water into chloride complexes exists and $[AuCl_3OH]$ has been observed.[4] While it is not possible to predict where the equilibrium lies, literature agrees on the initial formation of $[AuCl_2]^-$ by Cl^- adsorption and oxidation of gold.

7 Chloride Ion Concentration Dependence

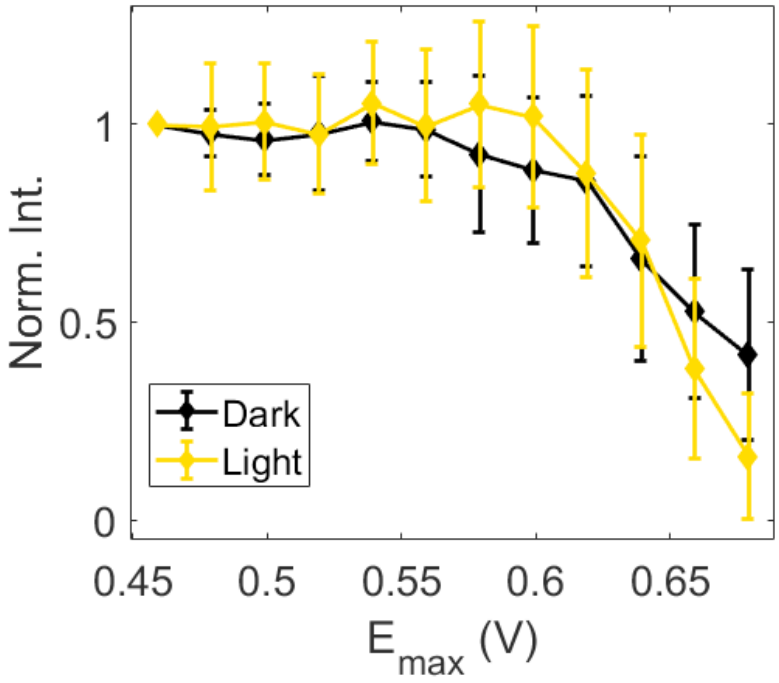

Figure 6. At a lower NaCl concentration (10 mM) the onset potential for electrodissolution is shifted to higher potentials. Plotted here is the average scattering intensity while stepping the potential up to 0.68 V in the dark (black, 23 particles) and in the light (yellow, 24 particles).

8 No Dissolution Under Illumination Only

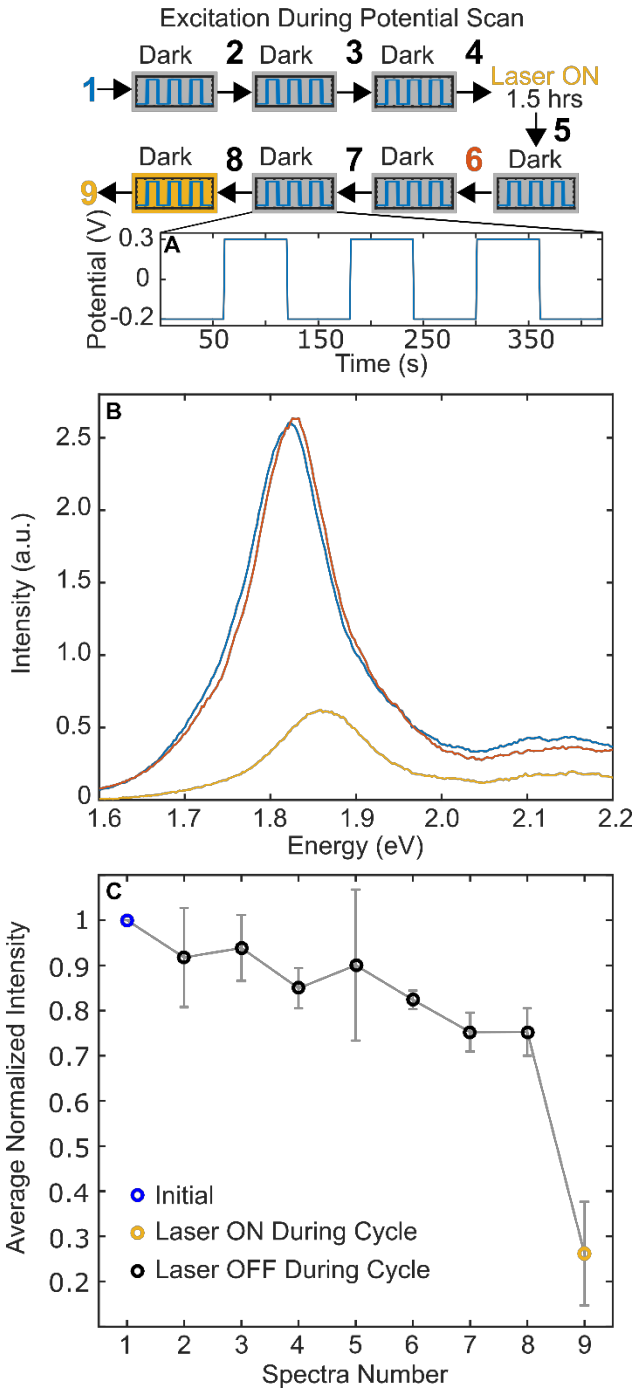

Figure 7. Change in scattering intensity while cycling an electrochemical potential in the dark before and after exposure to 19 kW cm^{-2} white light laser excitation to simulate the influence of

laser induced heating. (a) An initial spectrum was taken (1) followed by three potential cycles (2-4) from 0 to +0.51 V without illumination, followed by white light laser excitation but without applying the potential for 1.25 hours, and another spectrum (5) before continuing with three more potential cycles in the dark (6-8), and finally a last cycle with laser excitation (9). (b) Initial single nanorod scattering spectrum (1, blue), scattering spectrum after three potential cycles and separate 1.25 hours of white light laser irradiation (5, orange), and scattering spectrum after three potential cycles followed by one cycle under white light laser excitation. (c) Average normalized intensity of 8 nanorods for spectra taken at the steps indicated in (a). These studies clearly show that that nanorods did not dissolve without potential under illumination.

9 Excitation Wavelength Dependence

The absorption cross-section for a 35 x 75 nm gold nanorod was calculated using finite difference time domain (FDTD) simulations using Lumerical (Fig. S8). The substrate was modeled as an ITO layer with the thickness of 140 nm on a glass slide with a refractive index of 1.52. The entire structure was placed in a water background medium with a refractive index of 1.33. The relative number of photons absorbed with red and green light was calculated by multiplying a measured laser spectrum (Fig. S9) with the simulated nanorod absorption spectrum. For green light, integration was performed up to 550 nm, while for red light all wavelengths above 600 nm were included. Without any filters in the beam path, the nanorods absorbed 5.5 times as many red photons compared to green photons. We used a 550 nm shortpass filter and the full laser power for green light. For red light, we used a 600 nm longpass filter and optical density filters of 0.6 and 0.1 in series to decrease the incident light by 80%. Under these conditions, the nanorods absorbed 1.1 times as many photons in the red compared to the green spectral region. We then multiplied the laser spectrum by the nanorod absorption spectrum and the photon energy at each wavelength to find the total energy absorbed under red vs. green illumination. Under the same experimental conditions as described, the nanorods absorbed 10% more energy under green illumination.

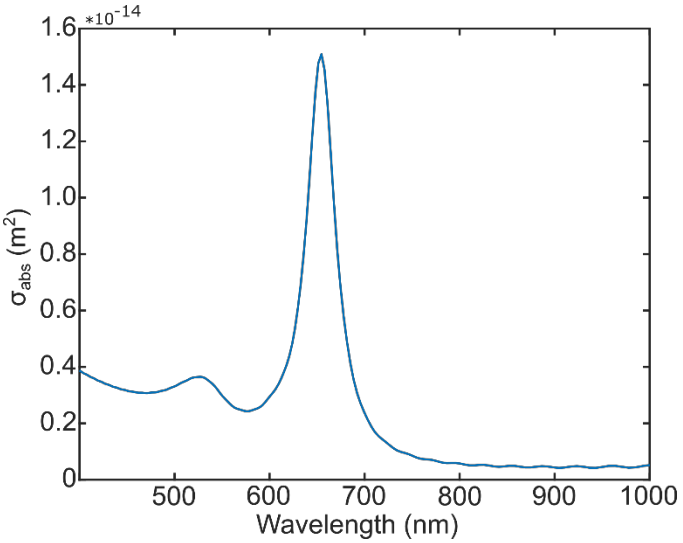

Figure 8. Simulated absorption cross-section for a 35 x 75 nm gold nanorod.

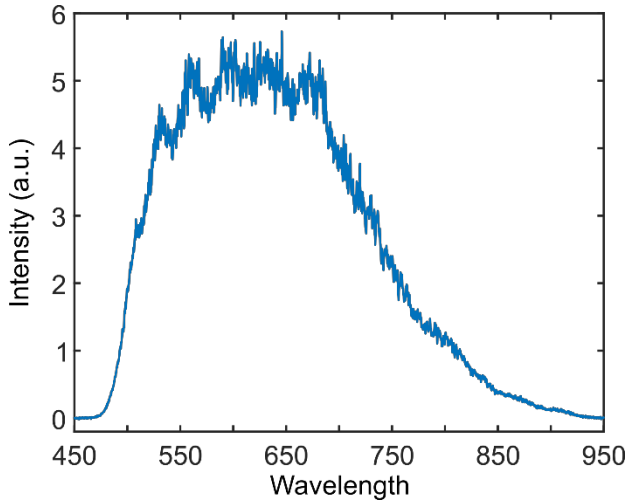

Figure 9. Measured white light laser spectrum.

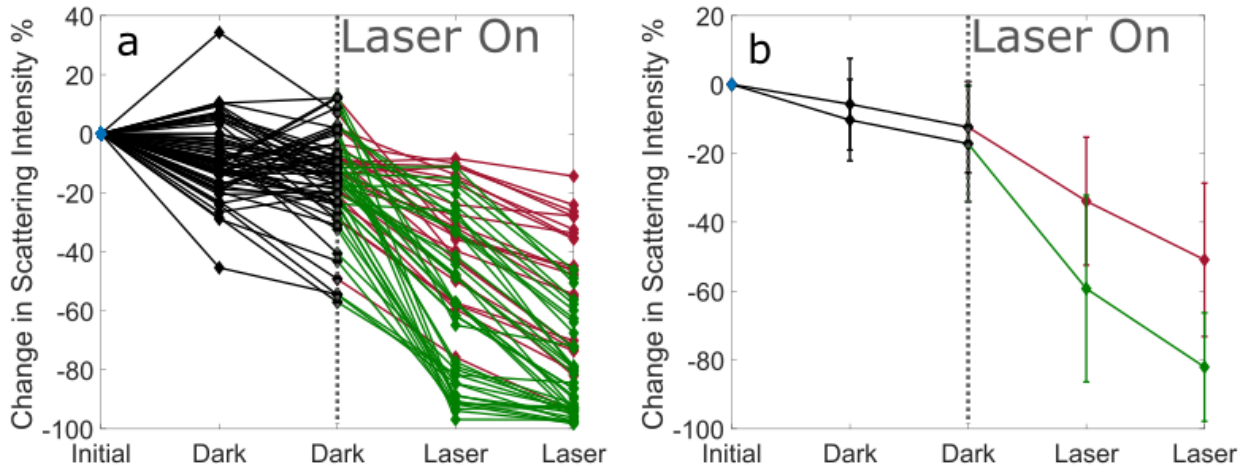

Figure 10. (a) Change in scattering intensity for single gold nanorods in the dark (black), under red light (red), and green light (green) illumination while cycling a 0.5 V electrochemical potential. The blue data point indicates the initial scattering intensity before a potential was applied. (b) Averaged values from (a) showing the mean with standard deviation.

A potential of 0.5 V was applied to nanorods for 2 cycles of 2 minutes each. The normalized difference between the initial intensity and the final intensity after the second cycle in the dark was used to create the cumulative distribution shown in Figure 3 (black line). The same nanorods were then illuminated with either red or green light and again 2 cycles of 0.5 V were applied for 2 minutes each. The normalized difference between the last cycle in the dark and the last cycle under illumination was used for the cumulative distributions in Figure 3 (red and green lines). Under these conditions, the same nanorods dissolve only slightly in the dark and more under green or red light illumination. The cumulative distributions for red and green light excitation includes data from 2 separate cells. The experiment was done in two separate areas on each cell. In one cell, the experiment was carried out using red light first, then green

light. For the other cell, the order was reversed. Both cells were calibrated using the ferricyanide/ferrocyanide redox couple.

10 Excitation Power Dependence

The change in scattering intensity was monitored at 0.53 V vs. SHE for 120 s under different laser intensities. The beam spot was held constant and different reflective neutral density filters (ThorLabs) were used to tune the power density. For each intensity, rates of scattering intensity decrease were found by applying a linear fit to the single particle trajectories of change in scattering intensity as a function of time, and then taking the mean. For the highest power of 13 kW cm^{-2}, linear fits were applied to the data collected during the first 40 seconds (first 20 data points). For all lower powers, linear fits were applied to the data collected during the first 100 seconds (first 50 data points) in order to ensure that only the linear portions of the scattering intensity decrease were considered. Temperature changes were calculated and ranged between 0.02 and 2 K. The linearity in rates of intensity decrease against incident power implies a hot carrier driven process, while an exponential dependence is expected for heating.[8]

Table 1. Conditions for the power dependence. Power density was calculated by dividing the measured white light laser power by the spot size obtained from a SLR camera image.

ND filter OD	**Power Density /kW cm^{-2}**	**Max. Heating /K**	**Slope s^{-1}**	**Number of particles**
No filter	13	2.04	1.27	10
0.3	6.5	1.02	0.61	12
0.6	3.3	0.51	0.38	13
1.0	1.3	0.20	0.07	18
2.0	0.1	0.02	0.01	8

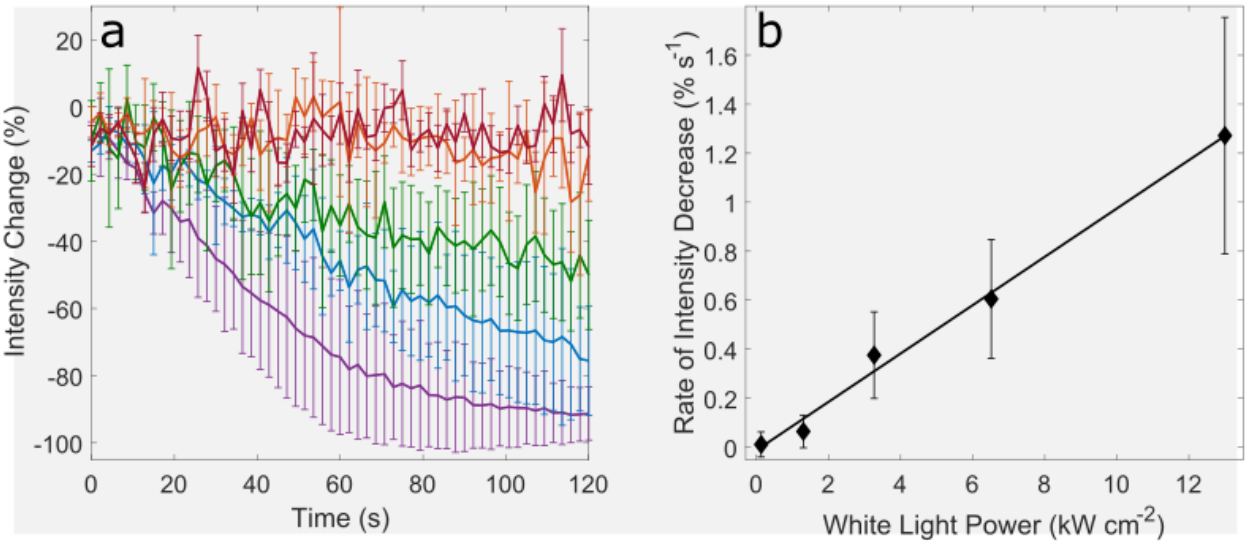

Figure 11: Excitation power dependence for the light assisted electrochemical dissolution of single gold nanorods. (a) Mean scattering intensity as a function of time while a potential of 0.53 V vs. SHE was applied under illumination with different white light laser intensities. Purple: 13 kW cm^{-2}, blue: 6.5 kW cm^{-2}, green: 3.3 kW cm^{-2}, orange: 1.3 kW cm^{-2}, red: 0.1 kW cm^{-2}. (b) Mean rate of intensity decrease against white light laser power with linear fit ($R^2 = 0.993$). The error bars indicate the standard deviation. For these experiments the entire white light laser spectrum (Fig. S9) was incident on the sample.

11 Plasmonic Heating Calculations

The change in the temperature at the surface of a plasmonic particle due to optical excitation, ΔT_{surf}, can be calculated according to:

$$\Delta T_{surf} = \frac{P_{abs}}{4\pi\kappa R} \qquad \text{(S1)}$$

where κ is the thermal conductivity of the material and R is the effective radius of the particle.[9, 10] The particle was assumed to be homogenously surrounded by water, with a κ of 0.6. This assumption leads to an overestimation of ΔT_{surf}, as ITO has a greater κ compared to water (11.0) and makes partial contact with the particle, leading to a reduced ΔT_{surf}. The excitation power absorbed by the particle, P_{abs}, is obtained from:

$$P_{abs} = \frac{\sigma_{abs} P_{heat}}{A} \qquad \text{(S2)}$$

where σ_{abs} is the absorption cross section of the particle, P_{heat} is the excitation power, and A is the size of the excitation beam spot. The white light laser power was 850 mW. Since a 900 nm dichroic short pass filter and a 1 cm by 1 cm cuvette filled with water was used to filter out longer wavelengths of light, the power was assumed to be distributed from 500 nm to 900 nm according to the white light laser spectrum shown in Fig. S8. The σ_{abs} for a 35 x 75 nm nanorod in water was calculated using FDTD simulations (Fig. S8). A SLR camera image was used to measure the beam spot (Fig. S1). A conservative estimate of the beam spot size was an ellipse with a 60 μm short axis and 176 μm long axis (Fig. S1). The ΔT_{surf} for a 35 x 75 nm gold nanorod under the white light laser excitation condition used in these experiments was then calculated to be 1.5 °C. While a local temperature increase should lead to an increase in the

dissolution rate,[11] this small temperature increase cannot explain the dramatic increase in the rate of intensity decrease observed with vs. without white light laser excitation.

12 Optical Heating Control

To ensure that white light laser heating of the electrolyte solution via water overtones or due to incomplete removal of IR irradiation did not influence the dissolution reaction, the white light laser was left on for 1.25 hours in between potential cycles (Fig. S7). If the white light laser dissolution enhancement was due to water heating, we would expect the next potential cycle (6, Fig. S7) to show a large decrease in scattering intensity. Instead, the scattering intensity decreased a similar amount compared to the previous cycles without white light laser excitation. A large decrease in scattering intensity due to dissolution was only observed with white light laser excitation during the last potential cycle (9). We also added a 1 cm path length cuvette filled with water to the excitation path, and measured a temperature increase for the water in the cuvette of 5 °C after 1 hour of continuous white light laser excitation using a thermocouple (HH 91, Omega). When a second cuvette was placed in the beam path, no temperature increase was observed in the second cuvette. We therefore conclude that the water cuvette filtered enough light to avoid heating our electrochemical cell.

13 Ligand Control

Since the spheres in Fig. S5 were spheres stabilized by citrate molecules and exhibit a similar behavior to the nanorods, we conclude that the ligands left over after O_2 plasma cleaning do not play a significant role.

References

1. Novo C, Funston AM, Pastoriza-Santos I, Liz-Marzán LM, Mulvaney P. Spectroscopy and High-Resolution Microscopy of Single Nanocrystals by a Focused Ion Beam Registration Method. *Angew. Chem. int. ed.* 2007, **46**(19)**:** 3517-3520.
2. Jing C, Rawson FJ, Zhou H, Shi X, Li WH, Li DW*, et al.* New Insights into Electrocatalysis Based on Plasmon Resonance for the Real-Time Monitoring of Catalytic Events on Single Gold Nanorods. *Anal. Chem.* 2014, **86**(11)**:** 5513-5518.
3. Hoener BS, Byers CP, Heiderscheit TS, Indrasekara ASD, Hoggard A, Chang WS*, et al.* Spectroelectrochemistry of Halide Anion Adsorption and Dissolution of Single Gold Nanorods. *J. Phys. Chem. C* 2016, **120**(37)**:** 20604-20612.
4. Gammons CH, Yu Y, Williams-Jones AE. The disproportionation of gold(I) chloride complexes at 25 to 200°C. *Geochim. Cosmochim. Acta* 1997, **61**(10)**:** 1971-1983.
5. Larios-Durán DSR-RaER. Electrochemical Study on Electrodissolution of Gold in Acidic Medium Using Chlorides as Ligands. *J. Electrochem. Soc.* 2017, **167:** 994-1002.
6. Kissner R. Halide catalysis of the electrochemical orddation of gold in acetonitrile. *J. Electroanal. Chem.* 1995, **385:** 71-75.
7. Diaz MA, Kelsall GH, Welham NJ. Electrowinning coupled to gold leaching by electrogenerated chlorine: I. Au(III) Au(I) / Au kinetics in aqueous Cl2/Cl− electrolytes. *J. Electroanal Chem.* 1993, **361**(1)**:** 25-38.
8. Yu Y, Sundaresan V, Willets KA. Hot Carriers versus Thermal Effects: Resolving the Enhancement Mechanisms for Plasmon-Mediated Photoelectrochemical Reactions. *J. Phys. Chem. C* 2018, **122**(9)**:** 5040-5048.
9. Gaiduk A, Yorulmaz M, Ruijgrok PV, Orrit M. Room-Temperature Detection of a Single Molecule's Absorption by Photothermal Contrast. *Science* 2010, **330**(6002)**:** 353-356.
10. Yorulmaz M, Nizzero S, Hoggard A, Wang LY, Cai YY, Su MN*, et al.* Single-Particle Absorption Spectroscopy by Photothermal Contrast. *Nano Lett.* 2015, **15**(5)**:** 3041-3047.
11. Gallego JH, Castellano CE, Calandra AJ, Arvia AJ. Electrochemistry of Gold in Acid Aqueous-Solutions Containing Chloride-Ions. *J. Electroanal. Chem.* 1975, **66**(3)**:** 207-230.